Underwater Binocular Meta-lens

Xiaoyuan Liu, Mu Ku Chen,* Cheng Hung Chu, Jingcheng Zhang, Borui Leng, Takeshi Yamaguchi, Takuo Tanaka,* and Din Ping Tsai*

Cite This: *ACS Photonics* 2023, 10, 2382−2389

**Read Online**

ACCESS | 📊 Metrics & More | 📖 Article Recommendations | 🗐 Supporting Information

ABSTRACT: Underwater optics in all-aquatic environments is vital for environmental management, biogeochemistry, phytoplankton ecology, benthic processes, global change, etc. Many optical techniques of observational systems for underwater sensing, imaging, and applications have been developed. For the demands of compact, miniaturized, portable, lightweight, and low-energy consumption, a novel underwater binocular depth-sensing and imaging meta-optic device is developed and reported here. A GaN binocular meta-lens is specifically designed and fabricated to demonstrate underwater stereo vision and depth sensing. The diameter of each meta-lens is 2.6 mm, and the measured distance between the two meta-lens centers is 4.04 mm. The advantage of our binocular meta-lens is no need of distortion correction or camera calibration, which is necessary for traditional two-camera stereo vision systems. Based on the experimental results, we developed the generalized depth calculation formula for all-size binocular vision systems. With deep-learning support, this stereo vision system can realize the fast underwater object's depth and image computation for real-time processing capability. Our artificial intelligent imaging results show that depth measurement accuracy is down to 50 μm. Besides the aberration-free advantage of flat meta-optic components, the intrinsic superhydrophobicity properties of our nanostructured GaN meta-lens enable an antiadhesion, stain-resistant, and self-cleaning novel underwater imaging device. This stereo vision binocular meta-lens will significantly benefit underwater micro/nanorobots, autonomous submarines, machine vision in the ocean, marine ecological surveys, etc.

KEYWORDS: *meta-lens, binocular vision, underwater depth sensing, stereo vision, deep learning*
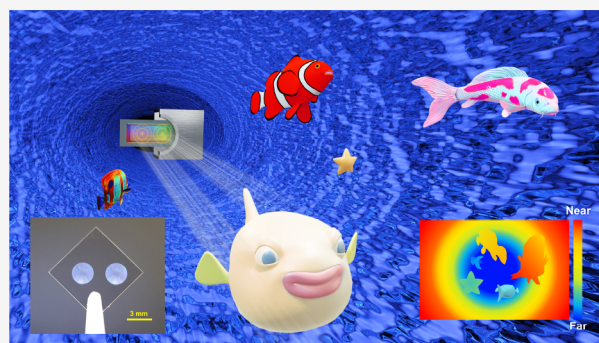
INTRODUCTION

The eyes are the primary organs for most animals to acquire visual information. In nature, there are many kinds of animals that have two eyes. It is well acknowledged that eagles are famous for their eyesight, and their eyes are among the best stereo vision in the animal kingdom.[1] Many of us have heard the phrase "eagle eye" to praise someone with sharp eyesight. Eagles are also fishing masters. For bald eagles, fish comprise about 70% of the year-round diet.[2] With excellent stereo vision, eagle can accurately judge the depth of underwater fish. The key to the eagle's super-stereoscopic sense is the highly overlapping binocular vision. When the left eye and right eye observe simultaneously, spatial offsets of the images are acquired. This offset is called binocular disparity. The magnitude of disparity is strongly related to the depth at which the object is viewed. Through disparity analysis, eagles can establish a three-dimensional perception of the scene. Such a binocular stereovision system is of great reference value for underwater machine vision.

The conventional binocular machine vision system is composed of two cameras. There is a complex data transformation to calibrate two-camera systems.[3] The complicated configuration leads to bulky physical size. Most importantly, measured objects may be inaccessible for bulky and sophisticated equipment in all-aquatic environments with limited and fragile space, such as underwater pipes, autonomous mini-submarines, and living organs. There is a strong demand for a miniaturized meta-device system for underwater imaging and sensing with all the needs of compactness, multifunction, durability, portability, lightness, etc., in all-aquatic environments. These demands are of great importance for the underwater optical science of environmental management, biogeochemistry, phytoplankton ecology, benthic processes, global change, etc.
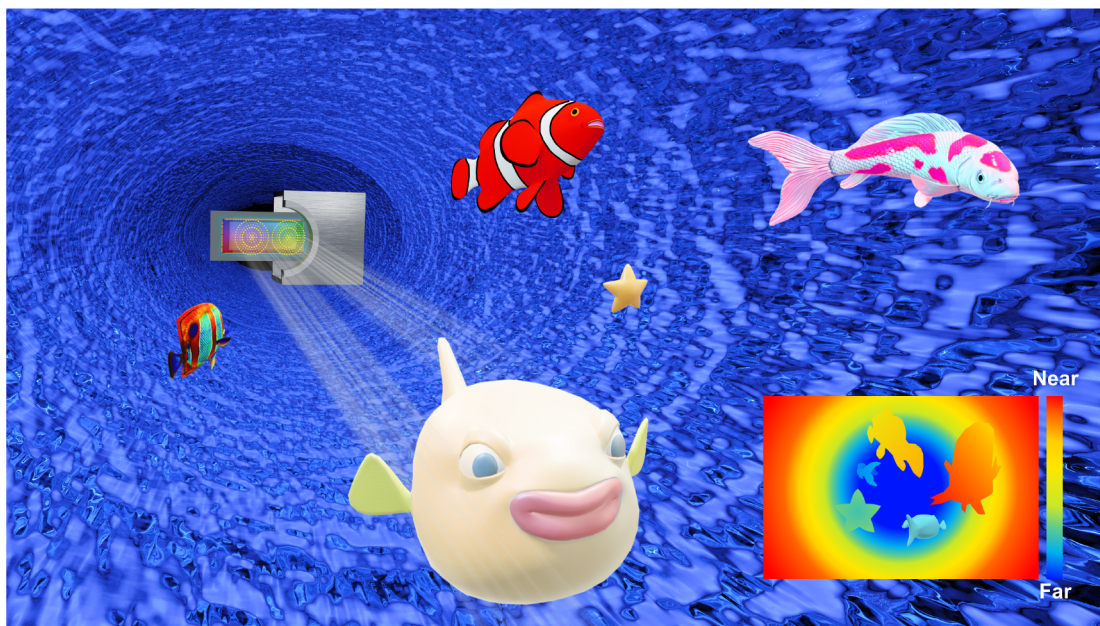
A meta-lens is an emerging flat optical device that can control and focus the wavefront of light by subwavelength nanoantennas.[4−9] Various nanoantennas with different structures can provide required modulations of phase, amplitude,

Figure 1. Scenario schematic of the underwater binocular meta-lens vision system. A pair of meta-lenses are fabricated on the same substrate and share one imaging CCD sensor. The disparities of binocular images can provide the depth of the imaging scene.

polarization, etc., for wide applications.[10−18] The design of the meta-lenses or the light field information process acquired by meta-lenses can be supported by artificial intelligence to realize specific functionalities or complex data analysis.[19−21] In the meantime, meta-lenses have the advantages of being light-weight and ultrathin, having a small footprint, having no spherical aberration, etc. There are some studies discussing depth-sensing systems based on meta-lenses. For example, the light field camera mimics the fly's compound eye for depth information through a large-scale meta-lens array,[22−24] and the trilobite-inspired bifocal light field camera provides a long depth of focus,[25] respectively. Some other indirect methods, such as imaging magnification,[26] dispersion characteristics,[27] and polarization transmittance imaging,[28] were also used for estimating an object's distance. However, previously reported results such as bifocal meta-lens learning from jump spiders to compute the depth via a point spread function (PSF)[29] and a double-helix PSF (DH-PSF) meta-lens[30−32] showed limited accuracy and range in depth sensing.

For extending the scenario of imaging and depth sensing for underwater targets, we implement underwater imaging with a binocular meta-lens device. Precise imaging, dense and accurate depth mapping, and compact configuration are necessary for underwater depth imaging research. For this demand, a pair of meta-lenses are specifically designed and fabricated on the same plane. The diameter of each meta-lens is 2.6 mm, and the centers of the two meta-lens are 4 mm apart. The focal length of two meta-lenses is designed to be 10 mm for the working wavelength of 532 nm. Because of the relatively large diameter of the meta-lens, no relay optical lens is required for our binocular meta-lens system. With no spherical aberration, our flat binocular meta-lens is located at the same plane, which is free of distortion correction and does not need system calibration. Considering the aquatic environmental conditions, we use GaN for our binocular meta-lens device. GaN is chemically and mechanically stable and has excellent endurance for extreme conditions. Our nano-structured GaN meta-lens is superhydrophobic, which is

suitable for underwater environments with antiadhesion, stain-resistant, and self-cleaning properties.

The scenario schematic of our underwater binocular meta-lens stereo vision is shown in Figure 1. Our binocular meta-lens is compact for working in a cramped and harsh aquatic environment. The system consists of a filter, binocular meta-lens, and a CMOS sensor. With captured images of a tube and multiple fish, the disparity imaging data are extracted through the matching algorithm, and the depth calculation formula can provide the stereo vision (Figure 1 inset at bottom right). Fast and accurate depth imaging can be acquired by our novel binocular meta-lens vision system.

■ METHODS

For the underwater stereo vision system, a monochromatic binocular meta-lens is designed and fabricated. In the design, the 532 nm light is modulated by the GaN cylindrical nanoantennas of the meta-lens. Each nanoantenna provides different phase modulation, which relates to the nanostructure geometry. The height of the nanoantenna is 750 nm, and the diameter varies from 90 to 196 nm with a period of 260 nm (see Supporting Information Figure S1). The polarization-independent phase modulation covers the 2π range by changing the diameter of the cylindrical GaN nanostructure. The data of phase shift and transmission intensity are derived from numerical simulation with the commercial software COMSOL Multiphysics. Different nanoantennas are arranged according to the focusing phase. The focusing phase profile is derived from eq 1.

$$\varphi(r, \lambda) = -\left[\frac{2\pi}{\lambda}\left(\sqrt{r^2 + f^2} - f\right)\right] \tag{1}$$

where $\varphi(r, \lambda)$ is the required phase at a distance away from the meta-lens center r under the working wavelength λ, and f is the designed focal length. The diameters of the two meta-lenses are 2.6 mm, and the designed focal length is 10 mm. The separation of two centers of the meta-lenses is 4 mm.
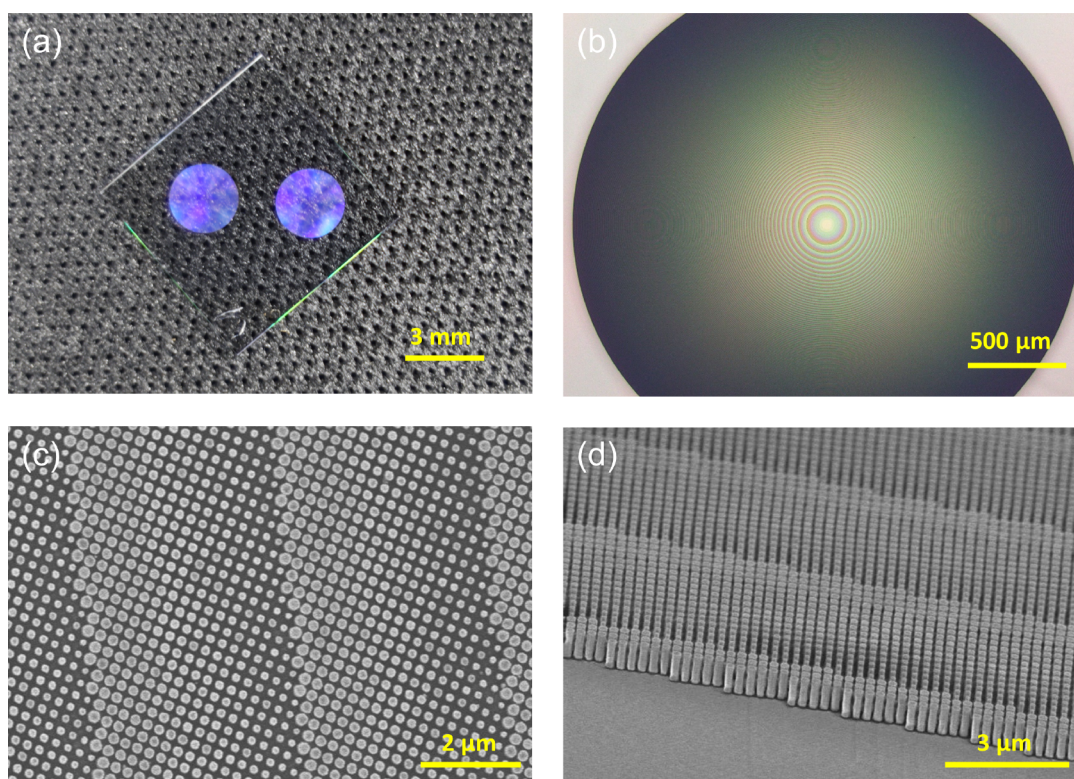
Figure 2. Optical and SEM images of the binocular meta-lenses and zoomed-in pictures. (a) Optical image of binocular meta-lenses fabricated on the substrate. (b) Optical photograph of one binocular meta-lens with a diameter of 2.6 mm. (c) The zoomed-in top-view SEM image. (d) The zoomed-in tilted-view SEM image at the edge of the meta-lens.

The binocular meta-lens is fabricated by the standard semiconductor microelectronics process using e-beam lithography (EBL) and several etching processes. A double-sided polished *c*-axis sapphire substrate is prepared for a 750 nm thick GaN layer grown using metalorganic chemical vapor deposition (MOCVD). A SiO_2 layer, 200 nm in thickness, is deposited on the GaN layer using an electron-gun evaporator. This SiO_2 layer is the hard mask for etching the high aspect ratio GaN nanostructures. A 200 nm thick positive photoresist, PMMA, is spin-coated onto the sample and baked at 180 °C for 3 min. The designed layout of the meta-lenses can be transferred to the photoresist layer by using the EBL system (ELS-HS50, ELIONIX INC.). After the e-beam writing, the sample is developed via a 1:3 methyl isobutyl ketone (MIBK)/ isopropyl alcohol (IPA) solution for 75 s and rinsed with IPA for 20 s. A Cr layer of 40 nm thick is deposited on the sample using an electron-gun evaporator. The lift-off process is performed in acetone to remove the photoresist. The layout is transferred to the Cr layer, which is the hard mask for etching the SiO_2 layer. The SiO_2 layer is etched by an inductively coupled-plasma reactive ion etching (ICP-RIE) system (Samco, RIE-200iPT) with CF_4 gas for transferring the pattern from the Cr mask. A chromium etchant can remove the residual Cr layer. The second ICP-RIE step, with a mixture of gas (Cl_2 and Ar), is used to form the GaN nanopillars with a high aspect ratio. The remaining SiO_2 mask layer can be removed by wet etching using a buffered oxide etch (BOE) solution. Finally, the needed GaN nanopillars remain on the sapphire substrate. Figure 2(a) shows the optical image of the binocular GaN meta-lens fabricated on a sapphire substrate. The bare eyes can well recognize two meta-lenses. Figure 2(b) is the optical picture of one of the binocular meta-lenses, which

is clean with a sharp edge. The specific cylindrical nanostructures can be observed by the scanning electron microscope (SEM), as shown in Figures 2(c) and 2(d). From the zoomed-in top-view SEM image in Figure 2(c), the cylindrical nanoantennas are well-defined and arranged according to the focusing phase profile. The zoomed-in tilted-view SEM image at the edge of the meta-lens shown in Figure 2(d) demonstrated the nanoantennas of our fabrication are sharply demarcated.

■ EXPERIMENTAL RESULTS AND ANALYSIS

Binocular Meta-lens. The focal length of two meta-lenses is measured and characterized (see Supporting Information Figure S2). A 532 nm wavelength continuous-wave laser beam is shaped into parallel light by a beam expander to cover the meta-lens fully. A motorized stage is adopted to control the image distance accurately. The focusing profiles of two meta-lenses on the $y-z$ plane are shown in the Supporting Information Figure S3. The measured focal lengths of the left and right meta-lenses are 9.994 mm and 9.996 mm, close to the designed focal length of 10.0 mm. By establishing a relative coordinate system, the separation of two meta-lens centers is measured at 4.041 mm. According to eq 2, the theoretical spatial resolution of the 0.13 numerical aperture (NA) meta-lens is 2.05 μm for the working wavelength of 532 nm.

$$\text{Spatial resolution} = \frac{0.5\lambda}{\text{NA}}, \quad NA = \frac{D}{2f} \quad (2)$$
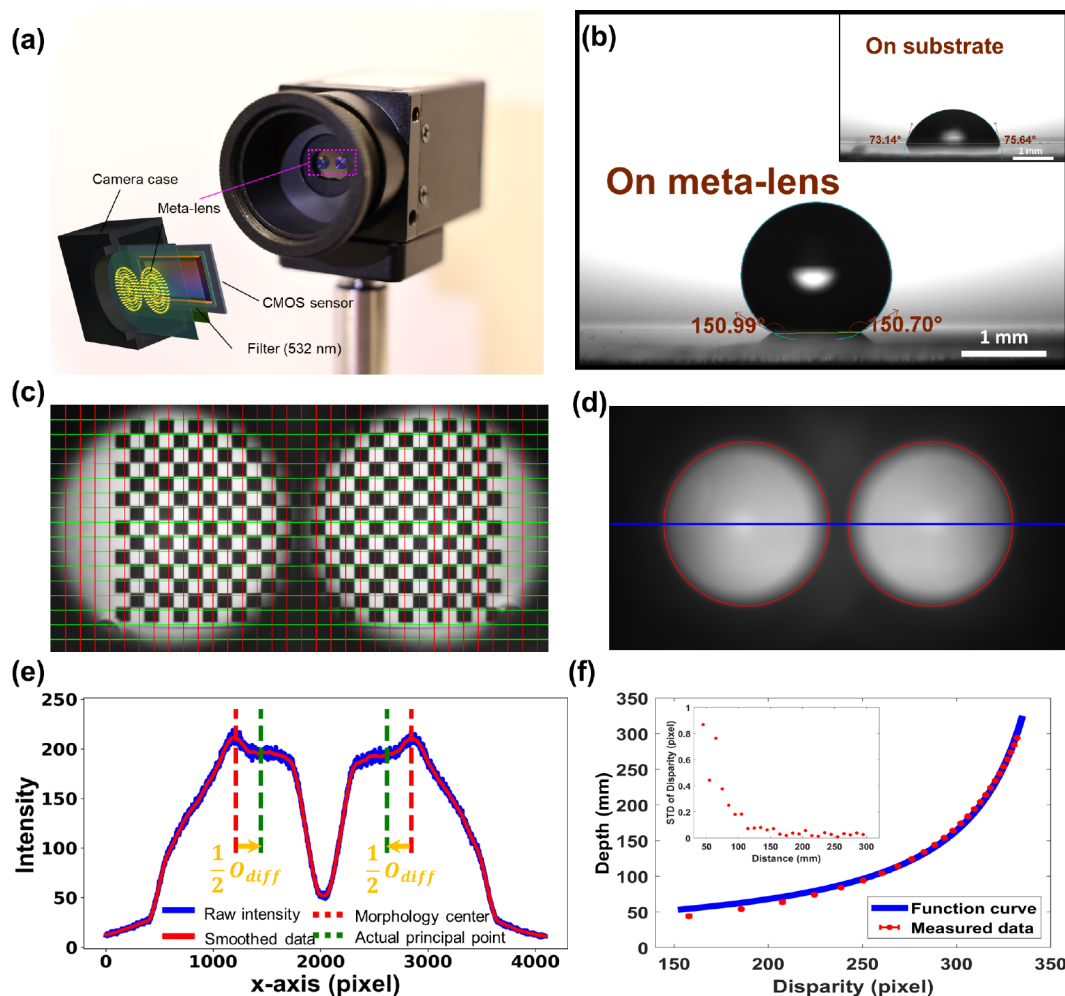
Figure 3. Performance analysis of the binocular meta-lens stereo vision system. (a) Photo of our binocular meta-lens system. The inset in the lower left is a sketch of the internal structure. (b) Photo of the contact angle of a water droplet on the surface of the meta-lens. Inset image in the upper right shows a water droplet's contact angle on the substrate's surface. (c) Picture of the checkerboard taken by our binocular system with horizontal (green) and vertical (red) lines. (d) Imaging range definition with morphological segmentation annotations by photographing a large bright object. Red circles annotate the imaging boundary. The blue line crosses the two principal points obtained by morphological analysis. (e) Intensity distribution along the blue line in (d). (f) Chart of an underwater disparity-depth function curve with measured data. The inset is the STD distribution of measured disparity.

, where λ is the working wavelength, NA is the numerical aperture, D is the diameter of the meta-lens, and f is the focal length.

The measured full width at half-maximum (FWHM) of the focal spot is 2.42 μm in both horizontal and vertical directions (see Supporting Information Figure S4). The experimental and theoretical values are in good agreement. Our binocular meta-lens can work in almost the entire visible region, 420−650 nm (see Supporting Information Figure S5). Measured focusing efficiency reaches 74% at the working wavelength of 532 nm. The focusing efficiency can be calculated by dividing the total light intensity of the focal point area at the focal length from the sample surface by the total light intensity of the meta-lens area (equal to the size of the meta-lens) at the sample surface. Focusing efficiency reflects the ability of the meta-lens to modulate the wavefront of incident light. The focusing performance in water is experimentally measured for our binocular meta-lens. The characterization comparison in air and water is reasonable, and the imaging capability of our meta-lens is close to the diffraction limit in water (see Supporting Information Figures S6−S8).

Spherical Aberration Free and Superhydrophobicity. Figure 3(a) displays our binocular meta-lens stereo vision system. It consists of a GaN binocular meta-lens, a color filter, and a CMOS sensor. The meta-lens can achieve focusing by modulating the phase and amplitude of the incident light with nanoantennas. The intrinsic property of the GaN nano-antennas is superhydrophobicity. Figure 3(b) shows the experimental measurements of the contact angles of a 3 μL water droplet at the surface of our GaN meta-lens and its sapphire substrate are 150.99° and 73.14°, respectively (see Supporting Information Figure S9 for experimental setup). The contact angle of a GaN surface usually is less than 90 deg.[33] Result of an over 150° contact angle demonstrates the superhydrophobicity of our GaN nanopillar structure. The superhydrophobicity properties of our nanostructured GaN meta-lens will enable an antiadhesion, stain-resistant, and self-cleaning[34] novel underwater imaging device, which is an advantage for underwater all-aquatic optical measurements. In the meantime, the nanoantennas' uniform height makes our meta-lens a flat optical component; that is, it is inherently free from spherical aberration. The imaging performance analysis of

our binocular meta-lens stereo vision system is displayed in Figures 3(c)−3(f). The image of the checkerboard shown in Figure 3(c) shows both of the auxiliary lines, horizontal lines in green and vertical lines in red, have no "bumps" or "depressions"; that is, there is no distortion. The imaging results of our binocular meta-lens demonstrate there is no spherical aberration. Usually, the traditional commercially available binocular cameras always need a complex coordinate system transformation to calibrate two image planes of two cameras. Two images must be strictly aligned in the horizontal direction so that the epipolar lines of the two images are exactly on the same horizontal line. In this way, any point on one image and its matching point on another image must have the same row number, and only a one-dimensional search on this row is needed to match the corresponding point. In our system, two meta-lenses are fabricated on the same substrate and share the same CMOS sensor. The epipolar lines of the two images are naturally on the same horizontal line (see green auxiliary lines in Figure 3(c)).

Generalized Depth Calculation Formula for All-Size Binocular Vision Systems. The traditional depth calculation formula of bulky commercial binocular lenses is

$$\text{dist} = \frac{fb}{\text{ps}^*(\text{disp} + d_{\text{offs}})} \tag{3}$$

, where dist is the depth from the object to the binocular lenses, f is the focal length, b is the baseline which is the separation distance of the centers of two lenses, ps is the physical pixel size of the sensor, disp is the computed disparity in pixel units, and d_{offs} is the x-offset of principal points caused by the misalignment of the lens and sensor chip. The principal point is the optical axis cross point at the image plane, also known as the image center. In a conventional and bulky camera system, the principal point is usually not exactly located at the sensor's center. In other words, the center of the CMOS sensor chip is not on the optical axis of the imaging lens. Therefore, commercial cameras usually provide two internal parameters, c_x and c_y, which are the x and y coordinate offsets relative to the principal point in the pixel coordinate system. When a binocular vision system uses two cameras with different internal parameters, i.e., the c_x are different, we can consider that the x-offset of two principal points of cameras is $d_{\text{offs}} = c_{x1} - c_{x0}$ (1 and 0 denote the left and right camera, respectively). In case two cameras are similar, i.e., $c_{x1} - c_{x0}$ and with no offset, the d_{offs} is 0. When two lenses simultaneously acquire the optical image information, in case their optical axes are not perpendicular to the imaging plane, we need to modify eq 3 as

$$\text{dist} = \frac{fb}{\text{ps}^*|\text{disp} + d_{\text{offs}} + O_{\text{diff}}|} \tag{4}$$

The additional term, O_{diff}, is the x-difference of principal point shifts caused by the tilts of the optical axes. O_{diff} varies with the image distance. To obtain the O_{diff} we can take a picture of a large bright object, as shown in Figure 3(d). The image with sharp exposure boundaries of the two lenses can be acquired. Threshold-based morphological analysis can yield the imaging boundaries of the two lenses, annotated as red circles in Figure 3(d). With the segmented boundaries (red circles), we can easily compute the morphological center coordinates of the two circular areas, which are (x_0, y_0) and (x_1, y_1). The morphological centers (image centers) are the principal points

of two lenses. When the binocular lenses are correctly aligned, y_0 will be equal to y_1. Cutting a line in Figure 3(d) along $y = y_1 = y_2$ (blue line), we can have the light intensity distribution as displayed in Figure 3(e). From Figure 3(e), we found the principal points are the apexes of the two intensity peaks. The separation of two principal points is

$$B = |x_0 - x_1|^*\text{ps} \tag{5}$$

, where x_0 is the x-coordinate of the left image center and x_1 is the x-coordinate of the right image center. The x-difference of principal point shifts O_{diff} can be shown in pixel unit by eq 6,

$$O_{\text{diff}} = \frac{b - B}{\text{ps}} \tag{6}$$

With this additional term, O_{diff}, eq 4 can be used for all-size and various configurations of the binocular lens system, i.e., a more generalized depth calculation formula.

For our binocular meta-lens stereo vision system, two meta-lenses share the common CMOS sensor. The image size is smaller than the sensor size. The coordinates of the principal point can be found by the morphological analysis. There is no misalignment problem between the lens and sensor. Therefore, d_{offs} is 0 for our binocular meta-lens system. The focal length of our meta-lens is 10 mm, the measured baseline is 4.041 mm, and the pixel size of the adopted CMOS sensor is 3.45 μm. The experimental imaging results provide us with the value of O_{diff}. We can experimentally verify eq 4 by conducting the underwater z-axis scanning measurements using our binocular meta-lens stereo vision system. A flat pattern board is placed in front of our binocular meta-lens and moves at 10 mm intervals from 44 mm to 294 mm. At each movement, one photo is taken for disparity computation. The average disparity of a region of interest (500 × 280 pixels) is recorded as one measurement data at a corresponding depth. Figure 3(f) shows the experimental results of depth versus disparity. The red dots are measured data with standard deviation (STD) error bars. The error bar is too short to be seen; therefore, an inset of STD distribution is provided in Figure 3(f). All the calculated STD values of disparity are less than 1 pixel. The measured STD values of depth are all less than 0.35 mm (see Supporting Information Figure S10). The small STD values indicate the measurements are stable and confident. To obtain the function curve of the depth calculation formula (eq 4) for this experiment, the term O_{diff} needs to be calculated. In the experiment, the coordinates of the two principal points in the pixel coordinate system are (1292, 1031) and (2834, 1031). According to eq 5 and eq 6, the calculated x-difference of principal point shifts, O_{diff}, is equal to −370.7 pixels. According to eq 4, we could have the function curve of the blue line shown in Figure 3(f). Results showed that all the measured data (red dots) are on the function curve (blue line). The experimental measurements agree with the generalized formula, eq 4. We have demonstrated that the generalized formula fits the all-size binocular stereo vision system.

Underwater Imaging and Depth Sensing. An underwater imaging and depth sensing experiment in the aquarium is conducted to test the three-dimensional imaging capability of our meta-lens stereo vision system (see Supporting Information Figure S11). Various marine toy animals are placed in different positions in the aquarium. We adopt the Pyramid Stereo Matching Network (PSMNet)[35] to process the binocular images for disparity computation. With the graphics
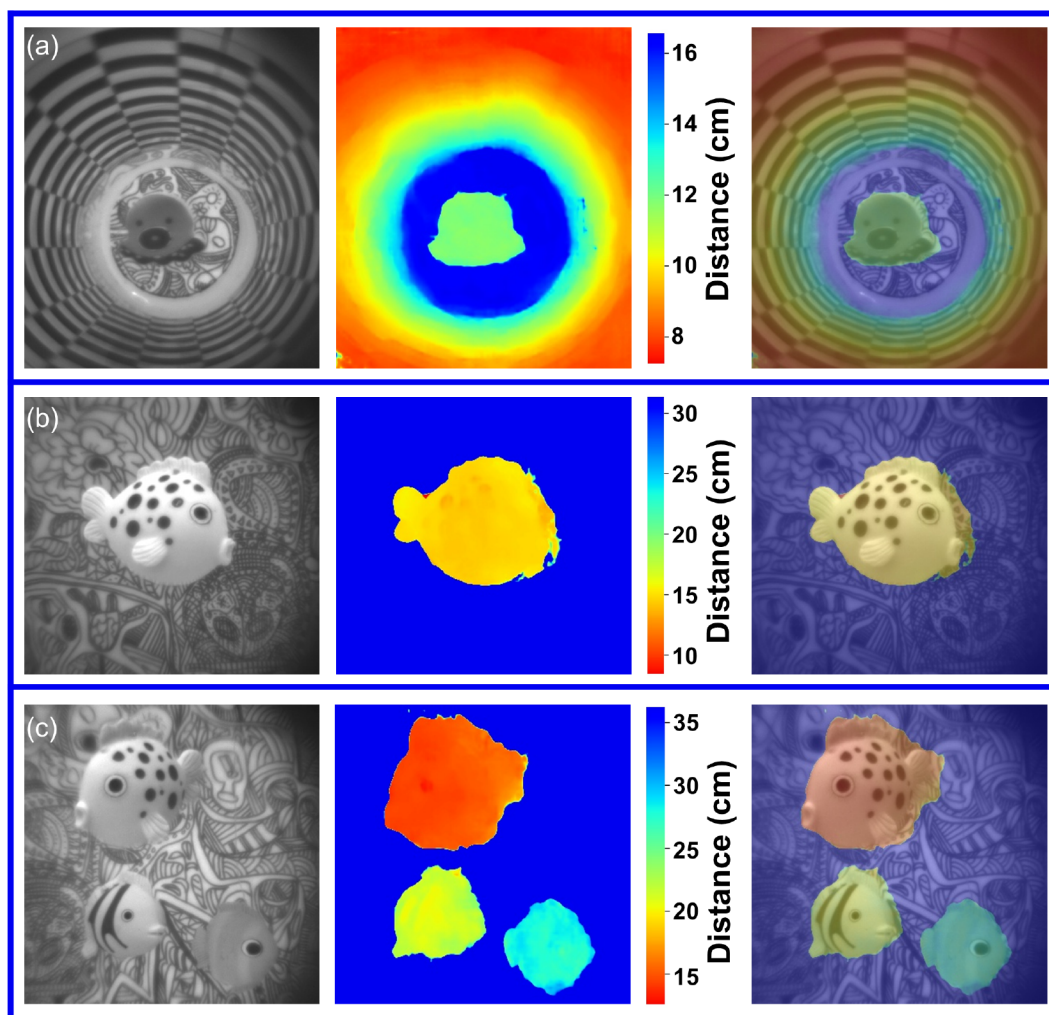
Figure 4. Underwater depth-sensing results. The left column is the raw image captured by the left meta-lens. The middle column is the depth map. The right column is the integration of two images. The depth map and the merged image share the color bar on the right. The depth is the distance from the object to the binocular meta-lens. (a) A tube ranges from 7.8 to 16 cm, and an octopus sticker is placed at a 12 cm distance. (b) A toy fish is located at a 15 cm distance. (c) Three toy fish are positioned at 14.5, 22, and 28 cm distances, respectively.

processing unit NVIDIA GeForce RTX 3080, the processing time is about 0.15 s. Compared with the conventional method of stereo block matching, their disparity computing capabilities are on par. The disparity computation results are both correct and fit the outline of the object (see Supporting Information Figure S12). However, the parameter adjustments are tedious in the conventional stereo block matching method. It may take a few minutes to acquire the best results. With comparable performance, the deep-learning method is better for real-time processing. Given the calculated disparity mapping, eq 4 could be used for the depth mapping. Figure 4 demonstrates corresponding underwater depth sensing results with deep-learning support. Three sets of images are shown in Figure 4, and each set is arranged from left to right as the raw image captured by the left meta-lens, depth mapping image, and the integration of two images. The integrated image is a superposition of 70% of the raw image intensity and 30% of the pseudocolor depth mapping. The purpose of integrated images is to show the edge fit for the raw and depth mapping images. The depth is the distance from the object to the binocular meta-lens. To simulate a narrow underwater channel scenario, we place a tube in the aquarium, as shown in Figure 4(a). The diameter of the tube is fixed. The pattern on the

inner wall of the tube reflects the imaging law of "everything looks small in the distance and large on the contrary". The tube in the image ranges from 7.8 to 16 cm, which agrees well with the depth-sensing result. An octopus sticker is placed in the tube 12 cm away from the binocular meta-lens. Figure 4(b) displays the scenario of a single toy fish placed at 15 cm. Figure 4(c) shows the multiobject scene, where three fish are placed at 14.5, 22, and 28 cm, respectively. From the depth mapping, all the depth-sensing results are correct. As shown in the merged image, the edges are also well-defined. Our binocular meta-lens can clearly distinguish underwater objects. Similarly, we also experimentally confirm the three-dimensional imaging and depth sensing of the scenario for the nonplanar object (i.e., even gradient depths can be accurately sensed), single object, and multiobject in the air (see Supporting Information Figure S13). All the experimental results demonstrated our binocular meta-lens stereo vision system is feasible for all-aquatic environments.

The distance from the binocular lens to the CMOS sensor is related to the computational accuracy limit. To have a clear and high-resolution image at a far distance from the binocular lens, the distance has to be small from the binocular lens to the CMOS sensor. The CMOS sensor should be at the focal length

for objects at infinity. Generally, the depths of our application scenario are much larger than the focal length. In eq 3 and eq 4, normally, the distance of the sensor could be approximated by focal length f, but the O_{diff} of eq 4 will be changed according to this distance. The accuracy limit decreases when this distance increases (see Supporting Information Figure S14). In our binocular meta-lens experimental measurements, the computational limit accuracy can reach 43.8 μm in the range where the sensor distance can be approximated as the focal length. In our experiments, results show an accuracy limit reaches 50 μm, which agrees well with the point spread function of our meta-lens in the optical axis (see Supporting Information Figure S15). For our binocular meta-lens system, the baseline, diameter of the lens, and numerical aperture are relatively small compared to the traditional and bulky camera lens, and the stereo vision model is susceptible to the shifts; that is, our binocular meta-lens system can provide a high sensing accuracy.

CONCLUSION

In this work, we demonstrate an optical underwater stereo vision system based on a novel binocular GaN meta-lens, which is specifically designed and fabricated. The system configuration is miniaturized and integrated. Our stereo vision system more flexibly matches various scientific and technical application scenarios than commercial binocular camera lenses. As a flat meta-optic device, there is no spherical aberration or image distortion. The design of the common substrate fabrication eliminates the tedious prerequisites of system calibration. GaN-based lens elements are stable in a wide variety of application environments and even extreme conditions. The intrinsic superhydrophobicity property of the nanostructured GaN meta-lens brings the advantages of antiadhesion, stain-resistance, and self-cleaning. We have developed the depth calculation formula for all-size binocular vision systems. Our stereo vision system can realize fast and intelligent depth imaging with deep-learning support. Three-dimensional imaging and depth sensing of a nonplanar object, single object, and multiobject were successfully implemented underwater or in the air. A 50 μm depth-sensing accuracy was demonstrated in experimental measurement results. We trust this novel meta-device with accurate three-dimensional imaging could be widely applied to underwater micro/nanorobots, autonomous mini-submarines, all-aquatic machine vision, marine ecological survey, etc.

ASSOCIATED CONTENT

Data Availability Statement

The data supporting this study's findings are available from the corresponding author upon reasonable request.

Supporting Information

The Supporting Information is available free of charge at https://pubs.acs.org/doi/10.1021/acsphotonics.2c01667.

> Design and characterization of the meta-lens, hydrophobicity of the GaN meta-lens, and experimental results of the underwater depth sensing (PDF)

AUTHOR INFORMATION

Corresponding Authors

Mu Ku Chen − *Department of Electrical Engineering, City University of Hong Kong, Kowloon, Hong Kong 999077; Centre for Biosystems, Neuroscience, and Nanotechnology and The State Key Laboratory of Terahertz and Millimeter Waves, City University of Hong Kong, Kowloon, Hong Kong 999077;* orcid.org/0000-0002-6697-0398; Email: mkchen@cityu.edu.hk

Takuo Tanaka − *Innovative Photon Manipulation Research Team, RIKEN Center for Advanced Photonics, Saitama 351-0198, Japan; Metamaterial Laboratory, RIKEN Cluster for Pioneering Research, Saitama 351-0198, Japan; Institute of Post-LED Photonics, Tokushima University, Tokushima 770-8506, Japan;* orcid.org/0000-0001-5714-5401; Email: t-tanaka@riken.jp

Din Ping Tsai − *Department of Electrical Engineering, City University of Hong Kong, Kowloon, Hong Kong 999077; Centre for Biosystems, Neuroscience, and Nanotechnology and The State Key Laboratory of Terahertz and Millimeter Waves, City University of Hong Kong, Kowloon, Hong Kong 999077;* orcid.org/0000-0002-0883-9906; Email: dptsai@cityu.edu.hk

Authors

Xiaoyuan Liu − *Department of Electrical Engineering, City University of Hong Kong, Kowloon, Hong Kong 999077;* orcid.org/0000-0001-5253-9313

Cheng Hung Chu − *Innovative Photon Manipulation Research Team, RIKEN Center for Advanced Photonics, Saitama 351-0198, Japan*

Jingcheng Zhang − *Department of Electrical Engineering, City University of Hong Kong, Kowloon, Hong Kong 999077*

Borui Leng − *Department of Electrical Engineering, City University of Hong Kong, Kowloon, Hong Kong 999077*

Takeshi Yamaguchi − *Innovative Photon Manipulation Research Team, RIKEN Center for Advanced Photonics, Saitama 351-0198, Japan;* orcid.org/0000-0002-7085-455X

Complete contact information is available at:
https://pubs.acs.org/10.1021/acsphotonics.2c01667

Notes

The authors declare no competing financial interest.

REFERENCES

(1) Grambo, R. L. *Eagles*; Voyageur Press, 2003.

(2) Armstrong, R. H. The importance of fish to bald eagles in southeast Alaska: A review. *Juneau, AK: Alaska Department of Fish and Game.* [Google Scholar] 2008.

(3) Cui, Y.; Zhou, F.; Wang, Y.; Liu, L.; Gao, H. Precise calibration of binocular vision system used for vision measurement. *Opt. Express* **2014**, 22 (8), 9134−9149.

(4) Sun, S. L.; Yang, K. Y.; Wang, C. M.; Juan, T. K.; Chen, W. T.; Liao, C. Y.; He, Q.; Xiao, S. Y.; Kung, W. T.; Guo, G. Y.; Zhou, L.;

Tsai, D. P. High-Efficiency Broadband Anomalous Reflection by Gradient Meta-Surfaces. *Nano Lett.* **2012**, *12* (12), 6223−6229.

(5) Nemati, A.; Wang, Q.; Hong, M.; Teng, J. Tunable and reconfigurable metasurfaces and metadevices. *Opto-Electron. Adv.* **2018**, *1* (5), 180009.

(6) He, Q.; Sun, S.; Xiao, S.; Zhou, L. High-efficiency metasurfaces: principles, realizations, and applications. *Adv. Opt. Mater.* **2018**, *6* (19), 1800415.

(7) Qiu, C.-W.; Zhang, T.; Hu, G.; Kivshar, Y. Quo vadis, metasurfaces? *Nano Lett.* **2021**, *21* (13), 5461−5474.

(8) Jung, C.; Kim, G.; Jeong, M.; Jang, J.; Dong, Z.; Badloe, T.; Yang, J. K.; Rho, J. Metasurface-driven optically variable devices. *Chem. Rev.* **2021**, *121* (21), 13013−13050.

(9) Sun, S.; He, Q.; Hao, J.; Xiao, S.; Zhou, L. Electromagnetic metasurfaces: physics and applications. *Adv. Opt. Photonics* **2019**, *11* (2), 380−479.

(10) Wang, Q.; Rogers, E. T.; Gholipour, B.; Wang, C.-M.; Yuan, G.; Teng, J.; Zheludev, N. I. Optically reconfigurable metasurfaces and photonic devices based on phase change materials. *Nat. Photonics* **2016**, *10* (1), 60−65.

(11) Zhao, M.; Chen, M. K.; Zhuang, Z.-P.; Zhang, Y.; Chen, A.; Chen, Q.; Liu, W.; Wang, J.; Chen, Z.-M.; Wang, B.; et al. Phase characterisation of metalenses. *Light Sci. Appl.* **2021**, *10* (1), 1−11.

(12) Zhang, X.; Li, Q.; Liu, F.; Qiu, M.; Sun, S.; He, Q.; Zhou, L. Controlling angular dispersions in optical metasurfaces. *Light Sci. Appl.* **2020**, *9* (1), 1−12.

(13) Wang, Q. H.; Ni, P. N.; Xie, Y. Y.; Kan, Q.; Chen, P. P.; Fu, P.; Deng, J.; Jin, T. L.; Chen, H. D.; Lee, H. W. H.; et al. On-Chip Generation of Structured Light Based on Metasurface Optoelectronic Integration. *Laser Photonics Rev.* **2021**, *15* (3), 2000385.

(14) Wang, R.; Intaravanne, Y.; Li, S.; Han, J.; Chen, S.; Liu, J.; Zhang, S.; Li, L.; Chen, X. Metalens for generating a customized vectorial focal curve. *Nano Lett.* **2021**, *21* (5), 2081−2087.

(15) Walter, F.; Li, G.; Meier, C.; Zhang, S.; Zentgraf, T. Ultrathin nonlinear metasurface for optical image encoding. *Nano Lett.* **2017**, *17* (5), 3171−3175.

(16) Chen, M. K.; Chu, C. H.; Liu, X.; Zhang, J.; Sun, L.; Yao, J.; Fan, Y.; Liang, Y.; Yamaguchi, T.; Tanaka, T. Meta-Lens in the Sky. *IEEE Access* **2022**, *10*, 46552−46557.

(17) Wei, S.; Cao, G.; Lin, H.; Yuan, X.; Somekh, M.; Jia, B. A varifocal graphene metalens for broadband zoom imaging covering the entire visible region. *ACS Nano* **2021**, *15* (3), 4769−4776.

(18) Sun, S.; He, Q.; Xiao, S.; Xu, Q.; Li, X.; Zhou, L. Gradient-index meta-surfaces as a bridge linking propagating waves and surface waves. *Nat. Mater.* **2012**, *11* (5), 426−431.

(19) Chen, M. K.; Liu, X.; Sun, Y.; Tsai, D. P. Artificial Intelligence in Meta-optics. *Chem. Rev.* **2022**, *122*, 15356.

(20) Lin, C.-H.; Chen, Y.-S.; Lin, J.-T.; Wu, H. C.; Kuo, H.-T.; Lin, C.-F.; Chen, P.; Wu, P. C. Automatic inverse design of high-performance beam-steering metasurfaces via genetic-type tree optimization. *Nano Lett.* **2021**, *21* (12), 4981−4989.

(21) Li, L.; Ruan, H.; Liu, C.; Li, Y.; Shuang, Y.; Alù, A.; Qiu, C.-W.; Cui, T. J. Machine-learning reprogrammable metasurface imager. *Nat. Commun.* **2019**, *10* (1), 1−8.

(22) Chen, M. K.; Liu, X.; Wu, Y.; Zhang, J.; Yuan, J.; Zhang, Z.; Tsai, D. P. A Meta-Device for Intelligent Depth Perception. *Adv. Mater.* **2022**, 2107465.

(23) Lin, R. J.; Su, V.-C.; Wang, S.; Chen, M. K.; Chung, T. L.; Chen, Y. H.; Kuo, H. Y.; Chen, J.-W.; Chen, J.; Huang, Y.-T.; et al. Achromatic metalens array for full-colour light-field imaging. *Nat. Nanotechnol.* **2019**, *14* (3), 227−231.

(24) Chen, M. K.; Yan, Y.; Liu, X.; Wu, Y.; Zhang, J.; Yuan, J.; Zhang, Z.; Tsai, D. P. Edge detection with meta-lens: from one dimension to three dimensions. *Nanophotonics* **2021**, *10* (14), 3709−3715.

(25) Fan, Q.; Xu, W.; Hu, X.; Zhu, W.; Yue, T.; Zhang, C.; Yan, F.; Chen, L.; Lezec, H. J.; Lu, Y.; Agrawal, A.; Xu, T. Trilobite-inspired neural nanophotonic light-field camera with extreme depth-of-field. *Nat. Commun.* **2022**, *13* (1), 2130.

(26) Liu, W.; Ma, D.; Li, Z.; Cheng, H.; Choi, D.-Y.; Tian, J.; Chen, S. Aberration-corrected three-dimensional positioning with a single-shot metalens array. *Optica* **2020**, *7* (12), 1706−1713.

(27) Tan, S.; Yang, F.; Boominathan, V.; Veeraraghavan, A.; Naik, G. V. 3D imaging using extreme dispersion in optical metasurfaces. *ACS Photonics* **2021**, *8* (5), 1421−1429.

(28) Zhao, F.; Lu, R.; Chen, X.; Jin, C.; Chen, S.; Shen, Z.; Zhang, C.; Yang, Y. Metalens-assisted system for underwater imaging. *Laser Photonics Rev.* **2021**, *15* (8), 2100097.

(29) Guo, Q.; Shi, Z.; Huang, Y.-W.; Alexander, E.; Qiu, C.-W.; Capasso, F.; Zickler, T. Compact single-shot metalens depth sensors inspired by eyes of jumping spiders. *Proc. Natl. Acad. Sci. U.S.A.* **2019**, *116* (46), 22959−22965.

(30) Jin, C.; Zhang, J.; Guo, C. Metasurface integrated with double-helix point spread function and metalens for three-dimensional imaging. *Nanophotonics* **2019**, *8* (3), 451−458.

(31) Colburn, S.; Majumdar, A. Metasurface generation of paired accelerating and rotating optical beams for passive ranging and scene reconstruction. *ACS Photonics* **2020**, *7* (6), 1529−1536.

(32) Jin, C.; Afsharnia, M.; Berlich, R.; Fasold, S.; Zou, C.; Arslan, D.; Staude, I.; Pertsch, T.; Setzpfandt, F. Dielectric metasurfaces for distance measurements and three-dimensional imaging. *Adv. Photonics* **2019**, *1* (3), 036001.

(33) Eickhoff, M.; Neuberger, R.; Steinhoff, G.; Ambacher, O.; Müller, G.; Stutzmann, M. Wetting Behaviour of GaN Surfaces with Ga-or N-Face Polarity. *Phys. Status Solidi (b)* **2001**, *228* (2), 519−522.

(34) Wu, Y.; Wang, Y.; Yang, W.; Song, Q.; Chen, Q.; Qu, G.; Han, J.; Xiao, S. Self-Cleaning Titanium Dioxide Metasurfaces with UV Irradiation. *Laser Photonics Rev.* **2021**, *15* (2), 2000330.

(35) Chang, J.-R.; Chen, Y.-S. Pyramid stereo matching network. In *Proceedings of the IEEE conference on computer vision and pattern recognition*; IEEE, 2018; pp 5410−5418.